Photogrammetric measurements of 3D printed microfluidic devices

Photogrammetric Measurements of 3D Printed Microfluidic Devices

Guerra M.G.[1], Volpone C. [1], Galantucci L.M. [1], Percoco G[1]

[1]Department of Mechanics, Mathematics, and Management, Polytechnic University of Bari, Viale Japigia, 182, 70126 Bari, Italy

Abstract

Additive manufacturing (AM) processes are being more frequently applied in several fields ranging from the industrial to the biomedical, in large part owing to their advantages which make them suitable for several applications such as scaffolds for tissue engineering, dental procedures, and 3D models to improve surgical planning. Moreover, these processes are particularly suited for the fabrication of microfluidic devices and labs-on-a-chip (LOC) designed to work with biological samples and chemical reaction mixtures.

An aspect not sufficiently investigated is related to the dimensional verification of these devices. The main criticality is the texture-less surface that characterizes the AM products and strongly affects the effectiveness of most currently available 3D optical measuring instruments.

In this study, a passive photogrammetric scanning system has been used as a non-destructive and lowcost technique for the reconstruction and measurement of 3D printed microfluidic devices. Four devices, manufactured with stereolithography (SLA), fused deposition modelling (FDM) a Stratasys trademark, also known as fused filament fabrication (FFF), and Polyjet have been reconstructed and measured, and the results have been compared to those obtained with optical profilometry that is considered as the gold standard.

Keywords: Microfluidics, 3D printing, Photogrammetry, Measurement.

1 Introduction

Additive manufacturing (AM) can be used to extrude metallic materials, hydrogels, or cell-loaded suspensions in order to incorporate functional components in microfluidic devices [1]. Traditional microfluidic manufacturing methods (i.e., soft lithography) require specialized fabrication skills and facilities, while AM is accessible and customizable to serve the needs of biology, chemistry, or pharma research and development [2]. Moreover, open source enables researchers to improve the design process and reduce production for specific applications [3].

Several interesting review papers have been dedicated to the topic of AM microfluidic devices such as [1,3–8]. These papers are focused on photo-polymerization-based additive processes but there is emerging evidence that extrusion-based processes could gain more importance in microfluidic applications owing to their inherent simplicity and versatility to accommodate well-defined materials along with their continuously evolving performance.

Together with the expansion of AM techniques, some questions have been raised. One of them is related to the measuring instruments capable of acquiring AM surfaces in order to perform dimensional verifications. Generally, little importance is given to the dimensional characterization of these devices. The most recent trend is to adopt non-contact methods, such as optical or x-ray techniques, instead of contact methods for dimensional verification, owing to their capability to acquire a large number of points in a short time [9]. In this context, numerous techniques have been developed that can be broadly classified into two categories: the passive (e.g., passive photogrammetry) and active methods (active photogrammetry, time of flight, and triangulation-based techniques). Active methods based on triangulation are more extensively studied and used for closerange measurement. Depending upon the nature of the structured patterns, these methods can achieve different spatial resolutions or accuracy, while fringe projection techniques use phase information to establish a correspondence that is typically robust regarding surface texture variations [10]. Most passive systems use one or multiple cameras, and image processing, to recreate the 3D form from a series of correlated images [11]. Active systems use their own light sources and recreate a 3D model of the object's form by detecting the modulation of projected illumination caused by the object's shape. The advantages of passive over active systems are that they are usually cheaper in terms of hardware requirements, lower in mass, more compact, and hence easier to use. However, they tend to be less accurate and slower compared to most active systems, and the post-processing algorithms play a fundamental role in the reconstruction process. Unlike active systems, which create an artificial texture on the object's shape, passive systems require textured surfaces in order to determine common features and hence relate multiple images taken at different positions on the object.

Recently, passive photogrammetry has been applied for the reconstruction of small objects with sub-millimetre features, proving that it is a promising alternative to other currently available optical methods. The main hurdle for the dimensional verification of AM parts is their texture-less surfaces, [11] especially those obtained with resins or plastic materials [12,13]. It is difficult for this technique to achieve high accuracy if an object surface does not have strong natural texture variations. A way to overcome this drawback, which affects the passive photogrammetric system, has been presented in [14] with the use of a laser speckle projection to obtain an active photogrammetry.

1.1 Additive manufacturing (AM) for micro fluidic devices

AM has recently raised interest as a way to fabricate microfluidic systems, owing to its automated, assembly-free 3D fabrication, rapidly decreasing costs, and fast-improving resolution and throughput. Indeed, injection moulding and soft lithography, routinely used to fabricate valves and pumps for fluidic automation, have high set-up and running costs, while additive manufacturing techniques are efficient because they (a) promote modular CAD design, (b) do not require tooling or assembly, (c) generate very little waste, and (d) reduce costs [15]. Among the AM processes, SLA has been widely applied to fabricate microfluidic devices because of its high accuracy and availability of relatively low-cost machines.

At first, SLA was used as a model for polydimethylsiloxane (PDMS) casting, such as in [16], where a micro-stereolithography 3D printer (Miicraft) was adopted to fabricate templates with a proprietary resin. Subsequently, the 3D-printed template was covered by PDMS, after protecting the surface of the template with a PDMS-compatible material. Subsequently, there has been a considerable amount of work focused on printing open microfluidic channels. This option is often chosen instead of printing enclosed channels because it is easier to remove the uncross-linked resin. In [2], a Miicraft printer was used to print a complex open microfluidic channel, which was then sealed with adhesive tape. The device was printed in the XY-plane, reducing both the surface roughness of the channels and printing time. This printing direction also exploited the resolution limit of the printer. Direct fabrication of transparent microfluidic devices with enclosed channels is also reported in [17], with square sections of side equal to 250 μm.

Moreover, FDM and FFF have gained market penetration in microfluidics recently, because of the finishing treatments, tuning of process parameters, increasing positioning accuracy, and reduction of available nozzle diameters. The existing approaches for the fabrication of microfluidic devices described in [14] using 3D printing are also applicable for FDM and FFF: (i) AM of templates for replicas of conventional materials (such as Polydimethylsiloxane-PDMS or Poly(methyl methacrylate)-PMMA); and (ii) direct AM of microchips, including open channels to be sealed and closed channels. One example of (i) is reported in [18], which used sacrificial FDM printing to create a complex 3D scaffold of cylindrical segments using organic ink, and subsequently embedded the scaffold with a UV-curable epoxy resin. By heating to 60 °C, the organic ink was thermally removed leaving the epoxy hollow geometry.

More recent examples of (ii) are reported in [19], such as the descriptions of reaction-ware devices by Cronin's group, using a 3D printer to initiate the chemical reactions and printing the reagents directly into a 3D reaction-ware matrix. Comparisons of photo-polymerization processes are reported in [20], where open channel devices were fabricated using a Form1 and compared to an i3DP drop-on-demand 3D printing machine (Shapeways Frosted Ultra Detail). The main interest of this

paper was the dimensional comparison, which was made qualitatively, using scanning electron microscope (SEMs) images to observe the smallest features manufacturable with both methods. To investigate the surface roughness of each printing method, SEMs images were taken from the two printed test pieces using both the fabrication methods.

1.2 Dimensional verification of micro fluidic devices

The measurement of micro-channels is a challenging task, as sectioning the device with a destructive procedure and analysing it with a microscope is the most popular method for their dimensional and geometric characterization. One of the most important non-destructive, quantitative inspection methods involves confocal sensors. Some examples of confocal sensors are the following: In [21] a confocal point sensor (CF 4) and a tactile roughness device (DEKTAK 3030) were used for measuring laser ablated channels in terms of ablation depth, wall-angle, and surface roughness. In [22], micro-channels were measured with a profilometer based on a confocal chromatic sensor and with a confocal microscope with higher lateral resolution. In [23], a comparison between the micromilled channels on electron beam melted (EBM) and direct metal laser sintered (DMLS) workpieces was reported, and scanning electron and confocal microscopes were the measuring instruments employed. Unfortunately, this kind of instrumentation suffers severe limitations when a highly sloped surface must be measured. In micro-channels, the micro-geometry retrieval of areas near vertical walls is important to better understand and predict the fluid flow. In this context, photogrammetry is capable of entirely reconstructing an object with any 3D shape, and could be applied to exploit its positive features. Close-range photogrammetry includes methodologies still under experimentation, which have developed considerably owing to their low cost, fast, and non-invasive scanning processes.

In the last years, photogrammetry has been used in several experiments to demonstrate its suitability for most dimensional ranges, down to sub-millimetric features [12,24–26] [27] [28]. Some of the aspects that limit its applicability, particularly in the case of sub-millimetric features, are related to the magnification level required, calibration pattern realization, and effectiveness of the camera calibration models. When high magnifications are required, the angle of view (AOV) becomes smaller and the depth of focus (DOF) gets narrower, leading to blurred images. The higher the magnification is, the smaller and more accurate the pattern used for camera calibration must be. Moreover, the pinhole camera model is theoretically effective under several assumptions that cannot be verified for millimetre and micro-scale applications. Another critical aspect, rarely treated in the research literature, regards the scale adjustment of the photogrammetric point clouds, as photogrammetry normally captures a model that must be scaled after processing.

Basically, using commercial software, the scale is retrieved through the following procedures [26]. In the first procedure, a known distance is measured between two codified markers within the

images [29–34], which is largely used for large-sized objects. However, small measurement volumes lead to a lower field of view with the following issues: (i) the markers must be smaller, resulting in increasing costs and technical problems for fabricating them; and (ii) blurring involves more extended image areas. In these conditions, marker detection becomes difficult. The second procedure consists in placing the camera(s) in known positions [23] [28] [35] or at a known distance between each other, as in traditional aerial photogrammetry, where each photo is geo-mapped through GPS. In [26], the scaling method finds the factor λ, under the hypothesis that the magnification ratio M of the camera is known with the considered extension tube and L, the lateral size of the pixel. The disadvantage of this method is the dependency on the operator. The operator's work consists of detecting non-blurred areas and computing the coordinates of two points on the images in these areas.

In the present study, a 3D passive photogrammetric measuring system has been adopted as a nondestructive and low-cost methodology for the reconstruction and dimensional verification of four AM micro-fluidic devices realized through SLA, FDM, FFF and Polyjet.

This paper is organized as follows. Section 2 describes the equipment involved during both the manufacturing and measuring processes. Emphasis is given to some aspects related to the lighting set-up adopted, which played an important role during the photogrammetric reconstruction, and to the scale adjustment procedure. In Section 3 the methodologies adopted to test the photogrammetric technique are described. In Section 4, the results are discussed before reaching the conclusions.

2. Materials and Methods

Figure 1 shows the micro fluidic device analysed as the target application. It was fabricated in four samples using the following machines for the corresponding processes: (i) stereolithographic Formlabs Form 2, (ii) FDM Stratasys F370, (iii) FFF Ultimaker 3, and (iv) Stratasys Objet 30 (Polyjet process). Table 1 reports the process details and parameters. These parameters are considered common practice parameters for each process typology.

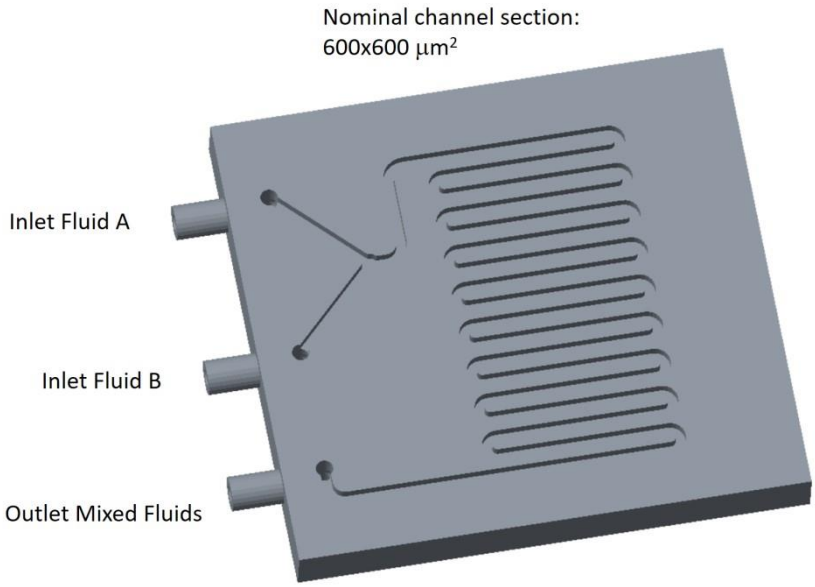

Figure 1 The analyzed AM microdevice (courtesy of Prof. Filippini)

3D printer model	**Printing method**	**Layer height (mm)**	**Laser spot size or nozzle diameter (mm) or resolution (DPI)**	**Filling or etching strategy**	**Type of material**
Formlabs Form 2	SLA, Stereolithography	0.025	0.14	solid	Clear Form V2 UV Photopolymer Resin
Stratasys F370	FDM, Fused Deposition Modeling	0.127	0.36	raster	Stratasys ABS
Ultimaker 3	FFF, Fused Filament Fabrication	0.090	0.40	raster	Ultimaker grey PLA

Stratasys Objet 30	Polyjet process	0.028	600 DPI (X and Y axes) 900 DPI (Z axis)	solid, glossy finishing	Vero White Plus UV Photopolymeric Resin

Table 1: 3D printers, process parameters, and materials used for the fabrication of the micro fluidic devices

The device is a micromixer consisting of two inlets, one outlet, and an 18-channel serpentine, which is able to mix two fluids in a laminar flow to achieve mixing by diffusion. The geometry has been chosen for its geometrical simplicity, being measurement of microchannels a complex task, especially referring to the sidewalls. Moreover, the choice of the fabrication technologies was based on some considerations. SLA and FDM-FFF are the most common technologies in microfluidics and in several other applications, while Polyjet is particularly promising for microfabrication owing to its inherent manufacturing accuracy.

From a 3D measurement point of view, these three technologies produce devices with interesting superficial features. Figure 2 shows the surface of each device captured with a Hirox RH2000 digital microscope equipped with MXB 5040RZ optics and set up to a magnification of 150x. The images in Figure 2 show the different aspects of the AM surfaces. SLA is not reflective, FDM and FFF are reflective (the white ABS more than the grey PLA) and characterized by evident beads, while Polyjet is reflective and with no evident beads.

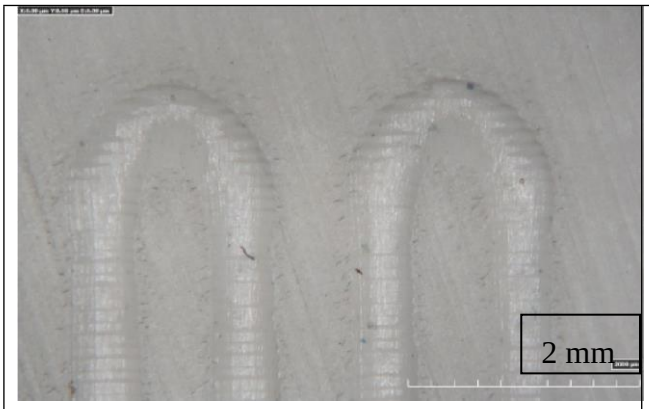

Figure 2a: Detail of the SLA micromixer

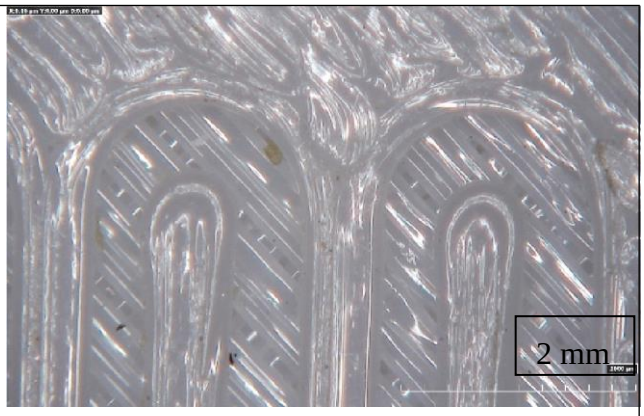

Figure 2b: Detail of the ABS-FDM micromixer

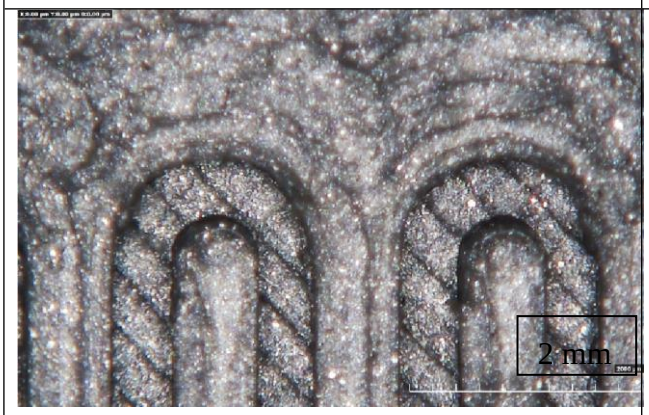

Figure 2c: Detail of the PLA-FFF micromixer

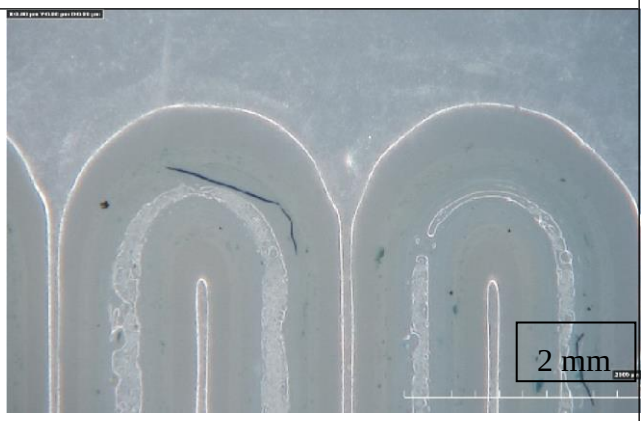

Figure 2d: Detail of the Polyjet micromixer

Figure 2 Images captured with a digital microscope.

2.1 Measuring system set-up

The experimental phase has been conducted using a full frame digital reflex camera (Canon Eos 6D) with a 20.2-megapixel resolution (5472 x 3648 pixel^2) and a full frame CMOS sensor (36 x 24 mm^2). A Canon EF 100mm f/2.8 macro lens, with the focus distance set to its minimum value, was used with a magnification ratio equal to 1:1 (Figure 3). This photogrammetric set-up has an optical ground resolution of 6.58 □m/pixel and a resolution depth of 13.16 □m/pixel, being respectively the (x,y) and z resolution of the photogrammetric system.

Generally, high performance measurements require the use of a calibration model in order to estimate internal parameters and lens distortions. Although, with modern structure-from-motion (SfM) approaches, the estimation of the internal parameters could be conducted without the use of traditional coded targets. It has been demonstrated that the SfM feature-based matching approach, coupled with automated photogrammetric network orientation, can yield camera calibration parameters of greater precision and equal accuracy of automatic self-calibration approach which involves the use of targets [36] [37]. A set of images depicting a scene with a good texture is sufficient for the extraction of natural corresponding image points. These are automatically matched with

feature-based approaches and robust estimation techniques. The successive photogrammetric bundle adjustment retrieves the unknown camera parameters and their theoretical accuracies. Target-less calibration has been implied in several recent researches with robust results, also if applied to small objects with sub-millimetric features. A necessary condition for the success of this procedure is the good quality of the images acquired, as well as the object texture with a huge number of recognizable features. In this work, preliminary tests were carried out using the SfM algorithm for internal calibration resulting in strong issues due to the texture-less surface of the 3D printed microfluidic devices. The surface did not allow the recognition of a sufficient number of common features among images. Thus, target-less camera calibration was not reliable and stable enough to be used in this context and the internal parameters were computed using the Agisoft Lens software which implements the Brown's model. Agisoft Lens is an automatic lens calibration software, which uses LCD screen as a calibration target. supports estimation of the full camera calibration It matrix, including non-linear distortion coefficients [38].

Agisoft Lens estimates the following camera calibration parameters:

• fx, fy - focal length

• cx, cy - principal point coordinates

• K1, K2, K3, P1, P2 - radial distortion coefficients, using Brown's distortion model

The use of an already calibrated lens made the 3D reconstruction more stable and repeatable. Furthermore, target-less calibration, in presence of few points, generally is more affected by uncertainties related to the image processing software [39]. The smooth and reflective surfaces of at least two of the four devices represented a significant challenge for the photogrammetric scanning system under scrutiny. To overcome this criticality, attention has been focused on the lighting conditions and a passive approach has been chosen, avoiding pattern projections and the increment of the mentioned issues. The system has been equipped with a small box with an LED strip that rotates together with a turning table and the object, so that variations of shadows and other light effects are minimized during the acquisition. For the same reason, another white LED source has been placed above the camera to minimize the influence of the environmental illumination and to create a more diffused light effect.

Moreover, each sample has been scanned with a different exposure time depending on its features. The illumination resulted to be critical for several reasons. PLA-FFF, the grey one, represented a challenge because the top surface and the microchannel bottom surface (darker than the top surface owing to the microchannel depth) required a different amount of illumination and a

different exposure time. This effect is not reported for the other samples owing to their lighter and more diffusive appearance, and their issues are mostly related to reflectivity. Figure 3 shows the white box illuminated on all sides with an LED strip integrated to the workpiece located at the centre of the box, which was positioned at the centre of a turning table ISEL-RFII with an angle accuracy of 0.16°. The rotation angle of the table was set at 5°; in fact, the smooth surfaces of the micro-mixers forced the use of a high number of images in order to increase the number of tie points recognized in the images, and thus, to allow the alignment and the whole reconstruction process. Finally, the camera has been tilted with respect to the table at 60°. This choice derives from previous experience [8] [23] [28]; a large tilt angle value, however lower than 60°, is preferable for objects with large depth values, such as deep holes, while for objects with smaller depth values, smaller tilt angles are appropriate.

For the experimental set up, three acquisitions for each device were carried out to evaluate the standard uncertainty owing to the measuring procedure. This parameter is of great interest, especially in this case, because of the dependence of the photogrammetric scanning system, as an optical instrument, on the environmental lighting conditions, which, together with the exposure time and the f/stop parameters, determine the quality of the final acquired image. The photogrammetric point cloud was achieved using Agisoft PhotoScan Pro version 1.2.6 [40].

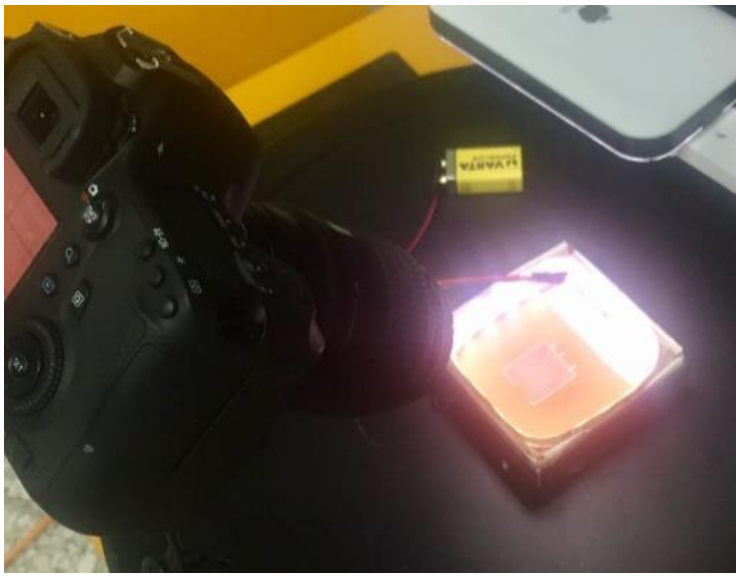

Figure 3 Experimental set-up

2.2 Scale Adjustment

One of the most important problems of the photogrammetric technique is the attribution of the scale to the reconstructed point clouds, owing to an inherent limitation of the technique. In this study, the scaling method described in [26] was employed. The scaling method proposed in that paper involved two parameters: the magnification level M, which is the ratio between the size of an object in the image and its true size; and the pixel size, which is a specification of the sensor used. The procedure consists of a series of subsequent steps. Firstly, two sets of photos of the workpiece must

be captured, each of which with a different diaphragm aperture. The diaphragm aperture is the parameter described by the f/stop value and it strongly affects the depth of field of the image captured. In this case, one aperture must be set to the largest value, f/2.8, because a larger aperture allows for easy recognition of the area most in focus in the image. The other aperture value must be set smaller. The latter value represents the best compromise between the depth of field and diffraction, and it has been set to f/20.

Starting from at least one image obtained with the largest aperture, two markers located in the most focused area have been identified, and the pixel distance measured (Figure 4). The distance in pixels is converted into millimetres through the magnification ratio M and the pixel size, according to Equations 1–5:

$$x_1[mm] = x_1[pixel] \cdot pixel\ size \quad (1)$$

$$y_1[mm] = y_1[pixel] \cdot pixel\ size \quad (2)$$

$$x_2[mm] = x_2[pixel] \cdot pixel\ size \quad (3)$$

$$y_2[mm] = y_2[pixel] \cdot pixel\ size \quad (4)$$

$$D_{12} = \frac{\sqrt{(x_2 - x_1)^2 + (y_2 - y_1)^2}}{M} \quad (5)$$

Where,

(x_1, y_1) are the coordinates of marker 1, and (x_2, y_2) are the coordinates of marker 2.

The *pixel size* refers to the lateral side of each pixel, and is a specification provided by the supplier, expressed in mm/pixel; D_{12} is the Euclidean distance, expressed in millimetres, between two points indicated with number 1 and 2; and M is the experimentally estimated magnification level. The measuring units are expressed in square brackets.

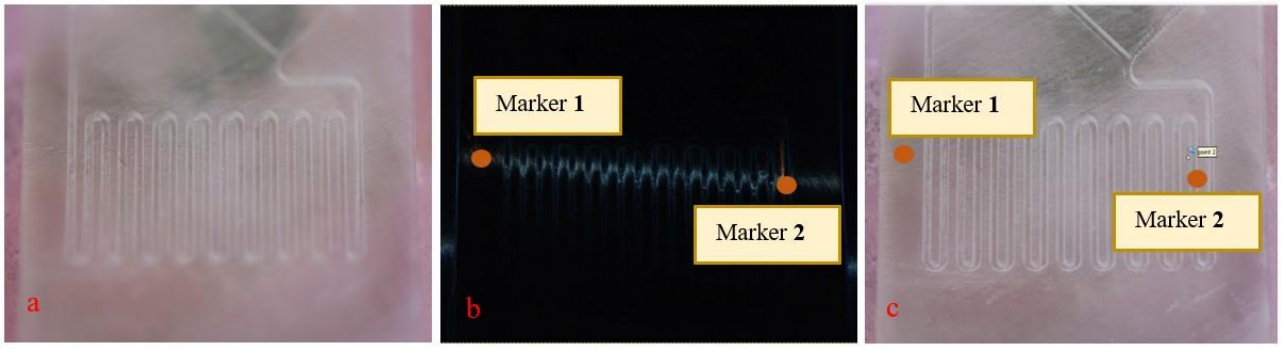

Figure 2 Scale procedure with two markers. a) image taken with f/2.8; b) image filtered to easily recognize the most focused part; c) image taken with f/20 used for the 3D reconstruction.

After this computation, the distances in millimetres were imported in the set of photographs with the smallest aperture value, which is the set of photographs that will be processed to obtain the final 3D model. This step allows to obtain a real scaled 3D model.

3. Results

Figure 5 depicts the photogrammetric reconstruction of the micro-mixers realized, respectively, with SLA, FDM, FFF and Polyjet. The photogrammetric measurements were compared to the point clouds obtained with the optical profilometer CCI-MP-HS TAYLOR HOBSON (OP) with a 20x-magnification lens, field of view of 0.8 x 0.8 mm2, a resolution of 1 □m, and a maximum slope of 17°. The global scanning time is approximately equal to 10 h for each device. Interferometry is one of the most popular techniques for the measurement of micro-channels owing to its capability to measure reflective and transparent objects. However, it does not allow the reconstruction of vertical sides, and the reconstructed part, after the removing of outliers, has a lower number of points than photogrammetry. The overall scanning time using photogrammetry is approximately equal to 4 h for each device.

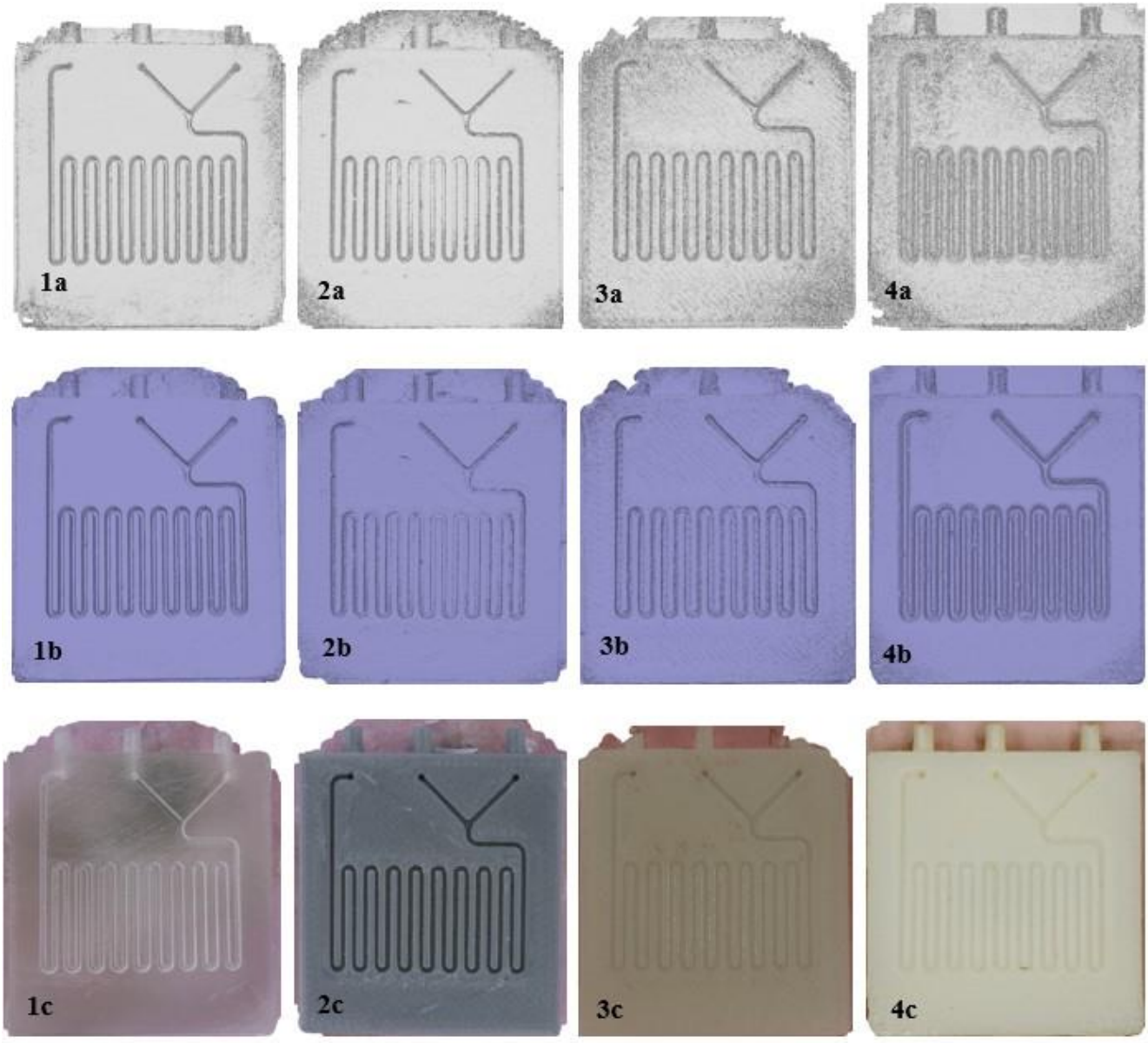

Figure 3 Devices reconstructed with photogrammetry. a) point cloud, b) mesh c) texturized mesh; SLA (1), PLA-FFF (2), ABS-FDM (3), Polyjet (4).

3.1 Point cloud comparisons

Point cloud comparisons were carried out with an open source Cloud Compare software (http://cloudcompare.org/). The comparison of point clouds, which are the first output of any optical instrument, avoids errors owing to the approximation of mesh and provides more accurate results. The average number of points reconstructed through the photogrammetric system depends on the sample reconstructed. The SLA and PLA-FFF registered the largest number of points, about 4,500,000, while the ABS-FDM and Polyjet registered a lower number of points, approximately 3,000,000. This is due to the smoother surface of the latter. Indeed, the number of points, which form the dense cloud, is directly affected by the number of points identified during the recognition phase.

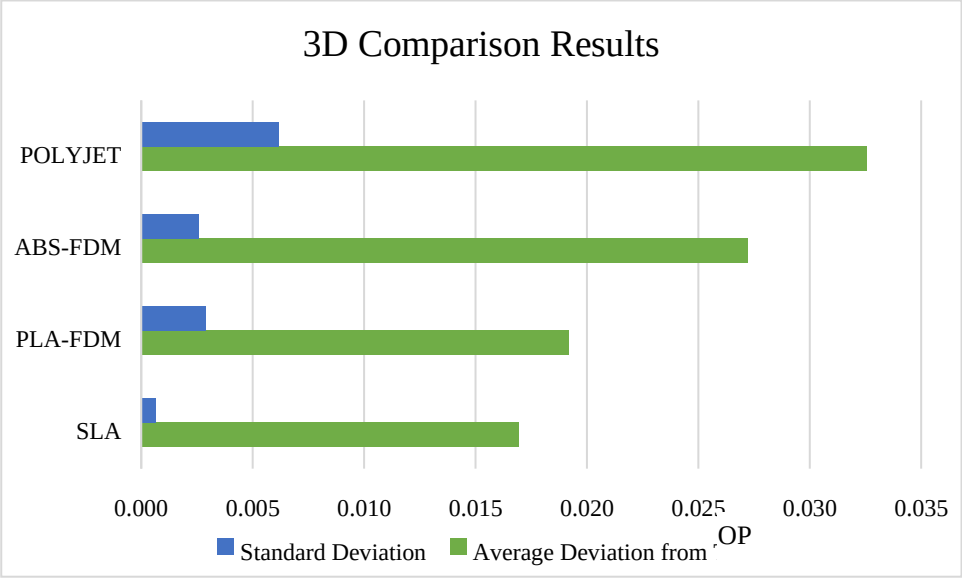

Figure 4 Point cloud comparison results using optical profilometer (OP)

In Figure 4, results from the 3D comparisons between the photogrammetric and the reference model (OP model) are reported in terms of average value of absolute distances between homologous points and in terms of standard deviation (σ) evaluated over three repetitions. These results provide initial evidence of the lower variability of the SLA measurements when compared to those of the FDM, FFF and Polyjet. Moreover, the average deviation must be discussed: the best performance was obtained with SLA, which has low reflectivity, while the most reflective, Polyjet, had the poorest performance, lower than 50 □m. Reflectivity affects the difference between FDM and FFF specimens, as the grey-PLA sample has much better performance than the white ABS. In every case, the performance of the photogrammetric technique with a passive approach is included in the interval of 17–33 □m. Considering that Formlabs (SLA) declares a laser spot size equal to 140 □m, the technique demonstrates a good performance when measuring these AM microfluidic components. SLA and PLA-FFF are thus the best candidates for dimensional verification by means of photogrammetry.

3.2 2D analysis results

Subsequently, a more detailed 2D analysis was conducted to provide the measure of depth for each of the 18 channels. A series of 100 profiles each were extracted for each considered model, and the medium profile was analysed with the TalyMap software to obtain the channel depth values. Figures 7–10 show the results of the measurements carried out using photogrammetry (PH) and the optical profilometer (OP), which is considered the gold standard with 1 □m of optical resolution. On the *x* axis, the 18 fluidic channels of each device are identified with a progressive number.

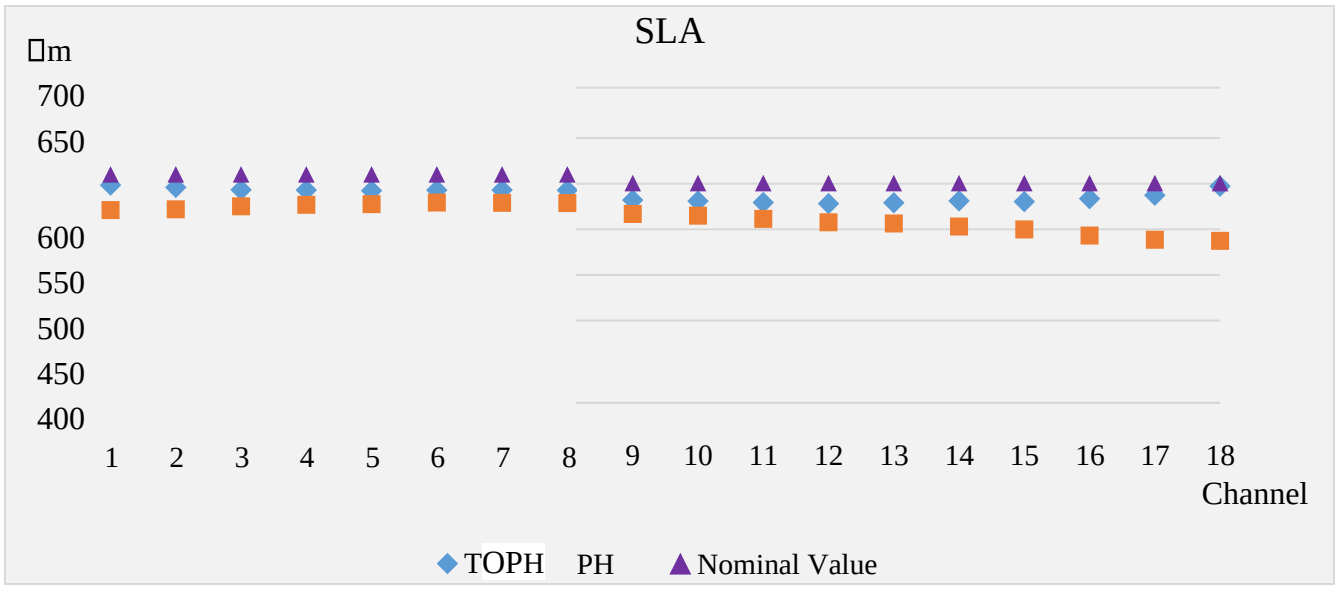

Figure 5 Measured depth values of SLA device 3D model, evaluated with Photogrammetry (PH) and optical profilometer (OP)

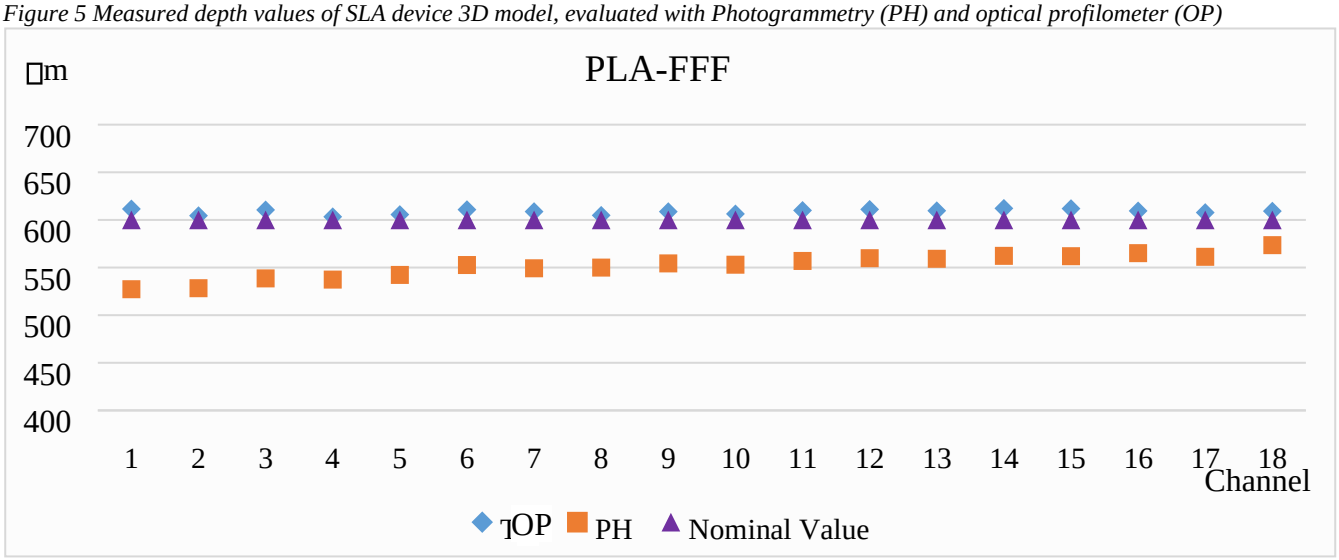

Figure 6 Measured depth values of PLA-FFF device 3D model, evaluated with Photogrammetry (PH) and optical profilometer (OP)

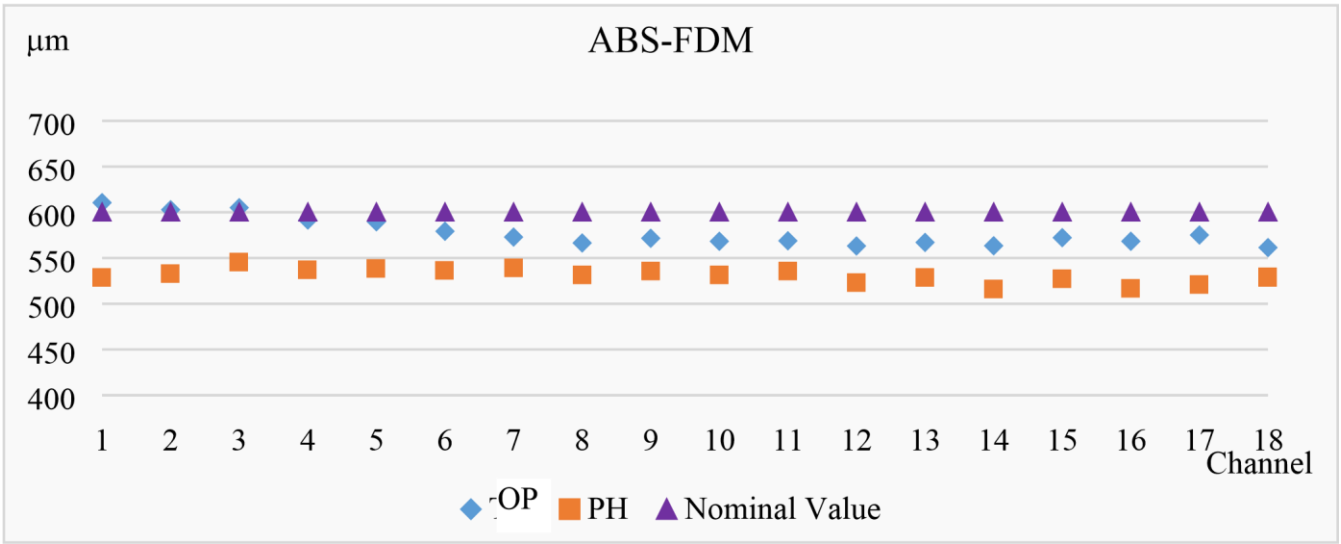

Figure 7 Measured depth values of ABS-FDM device 3D model, evaluated with Photogrammetry (PH) and optical profilometer (OP)

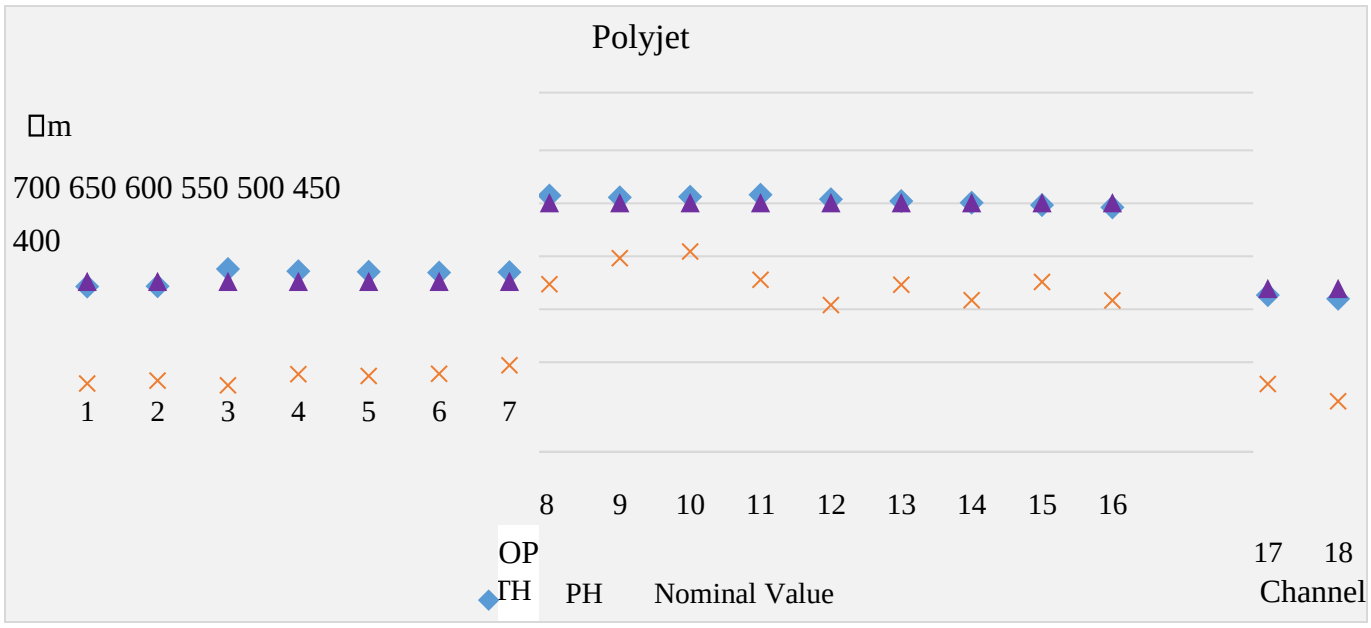

Figure 8 Measured depth values of Polyjet device 3D model, evaluated with Photogrammetry (PH) and optical profilometer (OP)

It is important to consider that the 3D STL model can differ significantly from measured point clouds, depending on the selected additive process. In fact, the results put in evidence these differences, highlighting the best dimensional performance of photopolymerization processes (Polyjet and SLA). However, the FFF process employing the PLA results in a very similar dimensional performance if compared to photopolymerization.

4 Discussion

The results obtained from the 3D comparisons between point clouds reveal the benefits and problems related to exploiting an optical technique, such as passive photogrammetry, to reconstruct transparent and reflective materials, typical of polymeric 3D printing.

The main advantage of a photogrammetric scanning system, which can be utilized for these kinds of measuring tasks, is its capability to reconstruct the whole model of the object, including the vertical walls, which represent a critical issue for most consolidated optical techniques. Other relevant advantages are the shorter time it requires for the acquisition with respect to optical profilometers, its simplicity, and the low cost of the scanning equipment.

Moreover, the texture-less surfaces and the criticalities caused by the reflection effect can be reduced by properly setting the lighting conditions in a way that allows the recognition of common points on the subsequent images.

Figure 11 reports the distribution of the deviation between homologous points on the photogrammetric models and that obtained with the OP. These graphs show that 95% of the PH points have an absolute distance with respect to the homologous OP points lower than 40 □m for SLA and PLA-FFF, 80 □m for ABS FDM, and 100 □m for the device realized with Polyjet.

The 3D models for the micro-mixers realized through SLA and FFF with grey PLA present minimum absolute distances (15 and 20 □m, respectively) when compared to the reference model, with more than 50% of the points within the range from 0 to 10 □m.

The Polyjet micro device is characterized by the maximum values of the absolute distance evaluated with respect to the reference model (up to 100 □m) in relation to the micro-channel depths. Moreover, the comparison was complicated owing to the small number of points measured with the optical profilometer, which makes it difficult to evaluate channel depths in a reliable way.

The results are strongly affected by the intended object textures, such as colour, transparency, and reflectance of materials. This feature complicates the task of recognizing a sufficient number of common features on the object, especially in correspondence to the micro channels.

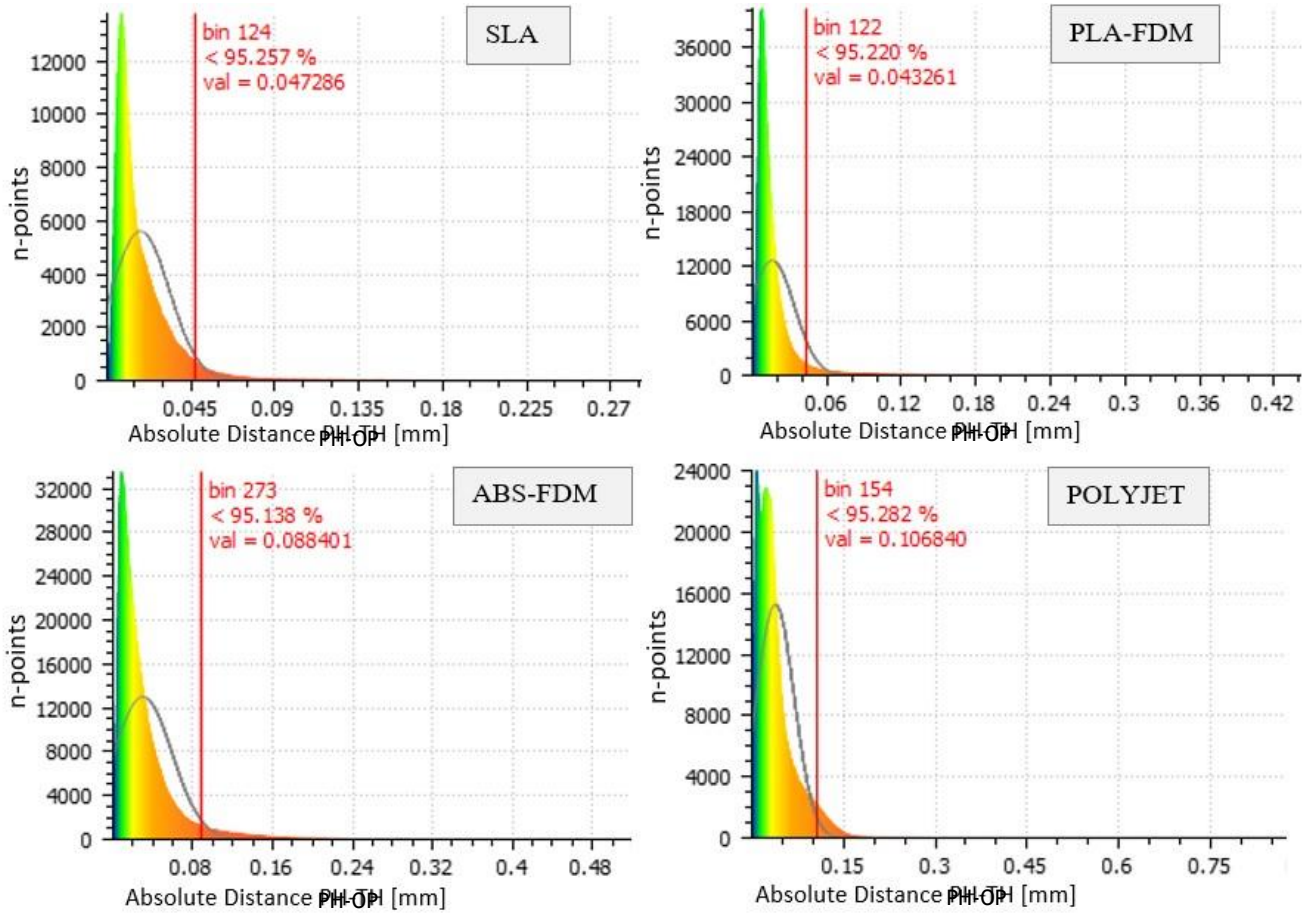

Figure 9 Histograms showing the point distributions with respect to the absolute distance between homologous points on the photogrammetric model and on the reference one.

In particular, the photogrammetric system was less sensitive to transparency, because the SLA device registered the best results in terms of 3D comparison and 2D analysis.

Another consideration is about the object dimensions and selected magnification level. The results show a data trend that leads to less deviation between the photogrammetric model and the reference model in relation to the channels located in the centre of the object. This area represents the most

focused part of the object. Indeed, the overall dimensions of the devices (about 33 x 28 x 3 mm^3) are about 50 times the channel depth values (0.6 mm), which means that the micro channels require a higher magnification level than that used for the entire object. Further investigations could be carried out to optimize the positioning of the markers for scale adjustment and, using a magnification level higher than 1x, to obtain a more detailed inspection of the micro-channel depths.

Furthermore, all the PH measures are smaller than the OP ones. This behaviour can be explained in different ways. Firstly, a possible scale error related to user-dependency of the scaling method adopted and the difficulty in focusing on the objects owing to their smooth and uniform textures. Secondly, the samples have not been scanned in a thermally controlled environment. Temperature variations are directly linked to systematic deviations that affect the measures. Polymeric materials have thermal expansion coefficients higher than those of metals (in the order of 70–150 × 10^{-6} K^{-1} for ABS and 85–100 *10^{-6} K^{-1} for PLA). In the near future, these aspects should be further investigated.

4.1 Standard uncertainty owing to measurement procedure, u_p

For each measure of depth, the uncertainty owing to the measuring procedure [41] has been computed, starting with the standard deviation obtained from the three scan repetitions [42].

$$u_p = \frac{S_x}{\sqrt{n}} \qquad (6)$$

Where:

S_x is the experimental standard deviation calculated as the square root of the variance, and n is the number of observations.

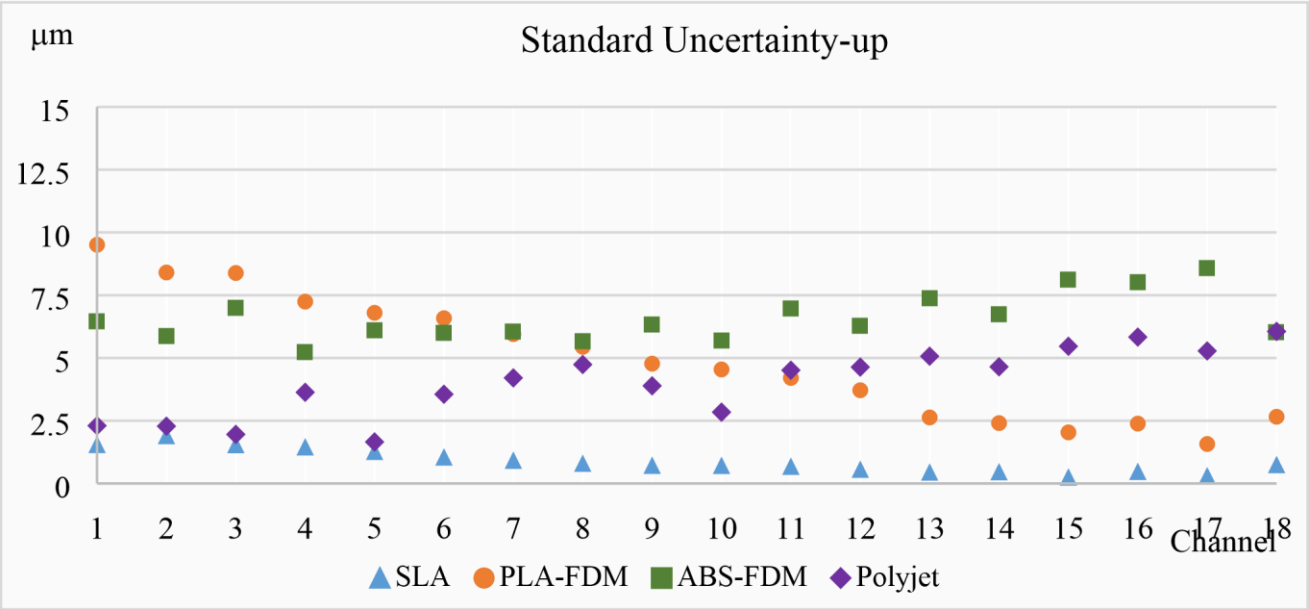

Figure 10 Uncertainty component owing to the measurement procedure

Figure 12 shows that the standard uncertainty, considering all the 18 channels, is below 2 □m for the SLA and below 10 □m for all the devices, when measuring channel sections equal to 600 × 600 □m^2. The reason of the different uncertainty values for different channels could be partially attributable to the variation of lighting conditions between subsequent sets of photographic images, and the low number of points reconstructed after the alignment phase, which increases the uncertainty component owing to the repeatability of the software[43].

Moreover, the thermal stability of polymeric materials represents a critical issue, and further analysis will need to be carried out to provide a more complete analysis regarding the correction of the systematic deviations caused by uncontrolled environmental temperature and the related uncertainty components.

5. Conclusions

In this paper, a photogrammetric scanning system has been used as a non-destructive and low-cost technique for 3D reconstruction and measurement of 3D-printed microfluidic devices. This task represents a challenge for most of the currently available non-contact measuring instruments owing to several factors, in particular the reflectance and transparency of these materials and their thermal and hygroscopic behaviour. Despite the unfavourable conditions caused by the reflectance and transparency of the devices, photogrammetry provided promising results. The device realized with SLA registered the minimum deviations, in the order of 10 □m, with a standard uncertainty of 1 micron.

The results seemed to be mostly affected by material reflectance (ABS-FDM and Polyjet), rather than material transparency (SLA). This makes this technique particularly suitable for the dimensional

verification of samples made via SLA, and the grey PLA also led to promising results. Furthermore, the location of the channels with respect to the object centre, which is the most focused area, seemed to influence the amount of deviation registered in relation to the OP models. Further investigations on the translucent FFF PLA, compared to the SLA resin, will be interesting. Moreover, further analysis will need to be carried out to improve the acquisition strategy by using higher magnification levels and more than just one focal point. Finally, the thermal and hygroscopic behaviour could be investigated in more detail to provide a systematic error compensation and an exhaustive uncertainty assessment.

6. Acknowledgements

The authors wish to thank Prof. Daniel Filippini (Linkoping University) for sharing the design of the micromixer, Dr. Piero Larizza and Dr. Daniela Pranzo (Masmec Biomed Inc.) for fabricating the Polyjet device, and Giuseppe Stolfa (Solfa IT Inc.) for fabricating the SLA devices.

7. References

[1] Au AK, Huynh W, Horowitz LF, Folch A. 3D-Printed Microfluidics. Angew Chemie - Int Ed 2016. doi:10.1002/anie.201504382.

[2] Morgan AJL, San Jose LH, Jamieson WD, Wymant JM, Song B, Stephens P, et al. Simple and versatile 3D printed microfluidics using fused filament fabrication. PLoS One 2016. doi:10.1371/journal.pone.0152023.

[3] He Y, Wu Y, Fu JZ, Gao Q, Qiu JJ. Developments of 3D Printing Microfluidics and Applications in Chemistry and Biology: a Review. Electroanalysis 2016. doi:10.1002/elan.201600043.

[4] Chen C, Mehl BT, Munshi AS, Townsend AD, Spence DM, Martin RS. 3D-printed microfluidic devices: fabrication, advantages and limitations-a mini review. Anal Methods 2016;8:6005–12. doi:10.1039/c6ay01671e.

[5] Ho CMB, Ng SH, Li KHH, Yoon Y-J. 3D printed microfluidics for biological applications. Lab Chip 2015;15:3627–37. doi:10.1039/C5LC00685F.

[6] Yazdi AA, Popma A, Wong W, Nguyen T, Pan Y, Xu J. 3D printing: an emerging tool for novel microfluidics and lab-on-a-chip applications. Microfluid Nanofluidics 2016;20:1–18. doi:10.1007/s10404-016-1715-4.

[7] Waheed S, Cabot JM, Macdonald NP, Lewis T, Guijt RM, Paull B, et al. 3D printed microfluidic devices: enablers and barriers. Lab Chip 2016;16:1993–2013. doi:10.1039/C6LC00284F.

[8] Amin R, Knowlton S, Hart A, Yenilmez B, Ghaderinezhad F, Katebifar S, et al. 3D-printed microfluidic devices. Biofabrication 2016;8:22001. doi:10.1088/1758-5090/8/2/022001.

[9] De Chiffre L, Carmignato S, Kruth J, Schmitt R, Weckenmann A. Industrial applications of computed tomography. CIRP Ann - Manuf Technol 2014;63:655–77. doi:10.1016/j.cirp.2014.05.011.

[10] Williams CB. The Status , Challenges , and Future of Additive Manufacturing in Engineering. Comput Des 2015;69:65–89. doi:10.1016/j.cad.2015.04.001.

[11] Stavroulakis PI, Leach RK. Stavroulakis , P . I . and Leach , Richard K . (2016) Review of post-process optical form metrology for industrial- grade metal additive manufactured parts . Review of 2016;87. doi:10.1063/1.4944983.

[12] Sims-Waterhouse D, Piano S, Leach R. Verification of micro-scale photogrammetry for smooth three-dimensional object measurement. Meas Sci Technol 2017;28:55010.

[13] Carmignato S, Aloisi V, Medeossi F, Zanini F, Savio E. CIRP Annals - Manufacturing Technology In fl uence of surface roughness on computed tomography dimensional measurements. CIRP Ann - Manuf Technol 2017;66:499–502. doi:10.1016/j.cirp.2017.04.067.

[14] Sims-Waterhouse D, Bointon P, Piano S, Leach RK. Experimental comparison of photogrammetry for additive manufactured parts with and without laser speckle projection. Proc. SPIE - Int. Soc. Opt. Eng., vol. 10329, 2017. doi:10.1117/12.2269507.

[15] Bhattacharjee N, Urrios A, Kang S, Folch A. The upcoming 3D-printing revolution in microfluidics. Lab Chip 2016;16:1720–42. doi:10.1039/C6LC00163G.

[16] Comina G, Suska A, Filippini D, Chen X, Hwang H, Nam S, et al. PDMS lab-on-a-chip fabrication using 3D printed templates. Lab Chip 2014;14:424–30. doi:10.1039/C3LC50956G.

[17] Moore B, Asadi E, Lewis G. Deposition methods for Microstructured and Nanostructured coatings on metallic bone implants: A review. Adv Mater Sci Eng 2017;2017. doi:10.1155/2017/5812907.

[18] Therriault D, White S, Lewis J. Chaotic mixing in three-dimensional microvascular networks fabricated by direct-write assembly. Nat Mater 2003.

[19] Symes MD, Kitson PJ, Yan J, Richmond CJ, Cooper GJT, Bowman RW, et al. Integrated 3D-printed reactionware for chemical synthesis and analysis. Nat Chem 2012;4:349–54. doi:10.1038/nchem.1313.

[20] Patrick WG, Nielsen AAK, Keating SJ, Levy TJ, Wang C-W, Rivera JJ, et al. DNA Assembly in 3D Printed Fluidics. PLoS One 2015;10:e0143636. doi:10.1371/journal.pone.0143636.

[21] Schille J, Schneider L, Loeschner U, Ebert R, Scully P, Goddard N et al. Micro processing of metals using a high repetition rate femtosecond laser: From laser process parameter study to machining examples. 30th Int Congr Appl Lasers Electro-Optics, ICALEO 2011 2011:773–82.

[22] Bulushev E, Bessmeltsev V, Dostovalov A, Goloshevsky N, Wolf A. High-speed and crackfree direct-writing of microchannels on glass by an IR femtosecond laser. Opt Lasers Eng 2016;79:39–47. doi:10.1016/j.optlaseng.2015.11.004.

[23] Rysava Z, Bruschi S. Comparison between EBM and DMLS Ti6Al4V Machinability Characteristics under Dry Micro-Milling Conditions. Mater Sci Forum 2016;836–837:177–84. doi:10.4028/www.scientific.net/MSF.836-837.177.

[24] Galantucci LM, Pesce M, Lavecchia F. A powerful scanning methodology for 3D measurements of small parts with complex surfaces and sub millimeter-sized features, based on close range photogrammetry. Precis Eng 2015. doi:10.1016/j.precisioneng.2015.07.010.

[25] Percoco G, Guerra MG, Sanchez Salmeron AJ, Galantucci LM. Experimental investigation on camera calibration for 3D photogrammetric scanning of micro-features for micrometric resolution. Int J Adv Manuf Technol 2017;91:2935–47. doi:10.1007/s00170-016-9949-6.

[26] Percoco G, Modica F, Fanelli S. Image analysis for 3D micro-features: A new hybrid measurement method. Precis Eng 2017;48. doi:10.1016/j.precisioneng.2016.11.012.

[27] M. GL, F. L, G. P. Multistack Close Range Photogrammetry for Low Cost Submillimeter Metrology. J Comput Inf Sci Eng 2013. doi:10.1115/1.4024973.

[28] Galantucci LM, Pesce M, Lavecchia F. A stereo photogrammetry scanning methodology, for precise and accurate 3D digitization of small parts with sub-millimeter sized features. CIRP Ann - Manuf Technol 2015;64:507–10. doi:10.1016/j.cirp.2015.04.016.

[29] Gallo A, Muzzupappa M, Bruno F. 3D reconstruction of small sized objects from a sequence of multi-focused images. J Cult Herit 2014;15:173–82. doi:10.1016/j.culher.2013.04.009.

[30] Luhmann T. Close range photogrammetry for industrial applications. ISPRS J Photogramm Remote Sens 2010;65:558–69. doi:10.1016/j.isprsjprs.2010.06.003.

[31] Ahmadabadian AH, Robson S, Boehm J, Shortis M, Wenzel K, Fritsch D. A comparison of dense matching algorithms for scaled surface reconstruction using stereo camera rigs. ISPRS J Photogramm Remote Sens 2013;78:157–67. doi:10.1016/j.isprsjprs.2013.01.015.

[32] Percoco G, Sánchez Salmerón AJ. Photogrammetric measurement of 3D freeform millimetre-sized objects with micro features: an experimental validation of the close-range camera calibration model for narrow angles of view. Meas Sci Technol 2015;26:95203. doi:10.1088/0957-0233/26/9/095203.

[33] González-Jorge H, Riveiro B, Arias P, Armesto J. Photogrammetry and laser scanner technology applied to length measurements in car testing laboratories. Meas J Int Meas Confed 2012;45:354–63. doi:10.1016/j.measurement.2011.11.010.

[34] Abbas MA, Setan H, Majid Z, Chong AK, Lichti DD. Improvement in measurement accuracy for hybrid scanner. IOP Conf Ser Earth Environ Sci 2014;18:12066. doi:10.1088/1755-1315/18/1/012066.

[35] Menna F, Sargeant B, Robson S. Improving automated 3D reconstruction methods via vision metrology. Proc SPIE - Int Soc Opt Eng 2015. doi:10.1117/12.2184974.

[36] Luhmann T, Fraser C, Maas HG. Sensor modelling and camera calibration for close-range photogrammetry. ISPRS J Photogramm Remote Sens 2016;115:37–46. doi:10.1016/j.isprsjprs.2015.10.006.

[37] Stamatopoulos C, Fraser CS. Automated Target-Free Network Orienation and Camera Calibration. ISPRS Ann Photogramm Remote Sens Spat Inf Sci 2014;II-5:339–46. doi:10.5194/isprsannals-II-5-339-2014.

[38] Agisoft Lens User's Manual n.d. http://downloads.agisoft.ru/lens/doc/en/lens.pdf (accessed April 5, 2016).

[39] Lavecchia F, Guerra MG, Galantucci LM. The influence of software algorithms on photogrammetric micro-feature measurement's uncertainty. Int J Adv Manuf Technol 2017:1–15. doi:10.1007/s00170-017-0786-z.

[40] Agisoft Photoscan User Manual 2016.

[41] ISO 15530-3:2011 Geometrical product specifications (GPS) -- Coordinate measuring machines (CMM): Technique for determining the uncertainty of measurement -- Part 3: Use of calibrated workpieces or measurement standards n.d.

[42] Lavecchia F, Guerra MG, Galantucci LM. Performance verification of a photogrammetric scanning system for micro-parts using a three-dimensional artefact: adjustment and calibration. Int J Adv Manuf Technol 2018;Accepted_p. doi:10.1007/s00170-018-1806-3.

[43] Lavecchia F, Guerra MG, Galantucci LM. The influence of software algorithms on photogrammetric micro-feature measurement's uncertainty. Int J Adv Manuf Technol 2017;93:3991–4005. doi:10.1007/s00170-017-0786-z.